The Journal of Chemical Physics

Ab initio complex potential energy curves of the $He^*(1s2p\ ^1P)$–Li dimer

Cite as: J. Chem. Phys. **152**, 184303 (2020); https://doi.org/10.1063/5.0008337
Submitted: 20 March 2020 . Accepted: 21 April 2020 . Published Online: 08 May 2020

Arie Landau, Anael Ben-Asher, Kirill Gokhberg, Lorenz S. Cederbaum, and Nimrod Moiseyev

The Journal of Chemical Physics ARTICLE scitation.org/journal/jcp

Ab initio complex potential energy curves of the $He^*(1s2p\ ^1P)$–Li dimer

Cite as: J. Chem. Phys. 152, 184303 (2020); doi: 10.1063/5.0008337
Submitted: 20 March 2020 • Accepted: 21 April 2020 •
Published Online: 8 May 2020

Arie Landau,[1,a] Anael Ben-Asher,[1] Kirill Gokhberg,[2] Lorenz S. Cederbaum,[2] and Nimrod Moiseyev[1]

AFFILIATIONS

[1]Schulich Faculty of Chemistry, Technion-Israel Institute of Technology, Haifa 3200003, Israel
[2]Theoretische Chemie, Physikalisch-Chemisches Institut, Universität Heidelberg, Im Neuenheimer Feld 229, Heidelberg D-69120, Germany

[a]**Author to whom correspondence should be addressed:** alandau@technion.ac.il. **Also at:** Theoretische Chemie, Physikalisch-Chemisches Institut, Universität Heidelberg, Im Neuenheimer Feld 229, Heidelberg D-69120, Germany.

ABSTRACT

LiHe is an intriguing open-shell dimer. It is an extremely weakly bound system, and its vibrational bound-state radius extends far into the classically forbidden regions. Exciting helium into 1*s*2*p* leads to a $^2\Sigma$ and a $^2\Pi$ state, in which lithium is in its ground state. These states are located above the ionization threshold of the Li atom, which makes them metastable, i.e., resonance states. Under these conditions, energy transfer between the atoms over large distances is feasible within the framework of interatomic Coulombic decay (ICD). These states are investigated theoretically; herein, we present and analyze the complex potential energy curves of the $^2\Sigma$ and $^2\Pi$ states, where their imaginary parts describe the decay rate of these resonance states. We employ the resonance via Padé approach to calculate these potentials. Thereby, we use the equation-of-motion coupled-cluster method to compute stabilization graphs as input data for the analytical dilation (via Padé) into the complex energy plane. The procedure is suitable for studying Feshbach resonances and ICD states such as the LiHe $^2\Sigma$ and $^2\Pi$ states. The resulting *ab initio* complex potential energy curves will be used in future work to describe the dynamics of the process $HeLi + h\nu \rightarrow He^*Li \rightarrow HeLi^+ + e_{ICD}$, which is amenable to experiment.

I. INTRODUCTION

Diatomic systems that include helium are the most weakly bound form of molecular matter, and they are bound due to the London dispersion forces that derive from the mutual induced-dipole–induced-dipole attraction (the weakest van der Waals force).[1,2] The existence of one of the most weakest bound pairs, He_2, was identified experimentally only in 1993,[3,4] while the existence of another such weakly bound pair, LiHe, was shown in 2013.[2] The two dimers, He_2 and LiHe, are quantum halo systems,[5] i.e., their bound state radius extends into the classically forbidden regions. A theoretical variational study of the LiHe $^2\Sigma$ ground state found a very shallow minimum (1.56 cm^{-1}) at 6.2 Å, which supports only one bound rovibrational state.[6] In addition, it was shown that the mean distance between the two atoms within $^7Li^4He$ and $^6Li^4He$ is about 29 Å and 50 Å, respectively.[6] The potential minimum of He_2 is five times deeper than that of LiHe, and its minimum distance is about twice smaller, but it has a very large average bond length of roughly 52 Å.[7] That is, these dimers spend most of the time in the classically forbidden region (beyond the confines of its potential). He_2 spends about 80% in the forbidden region and $^7Li^4He$ spends about 60% (and even more time in the $^6Li^4He$ case).[1] Consequently, these species have the potential to exhibit interesting quantum phenomena. In this paper, we theoretically investigate the lowest excited He^*–Li dimer.

An example of such a phenomenon was demonstrated, experimentally and theoretically, by Sisourat *et al.* for He_2.[8] As an extremely large quantum system, the two helium atoms can exchange energy over distances of more than 45 times their atomic radius.[8] The energy transfer process, in which the dimer is autoionized, is known as interatomic Coulombic decay (ICD)[9–11] (a key feature in ICD is the transfer of energy over large distances via a

virtual photon). ICD within He_2 occurs upon simultaneous ionization and excitation of one helium atom; the energy stored by this excited ion is transferred to the neighboring neutral helium atom and ionizes it. The excited ion relaxes by ICD to $He^+(1s)$, and the neutral helium is ionized to $He^+(1s)$ as well and emits the ICD electron. The resulting two $He^+(1s)$ then undergo a Coulomb explosion and fly apart.[8] Moreover, we wish to emphasize on the importance of such interatomic decay processes, which is not purely academic. It was demonstrated that they play a crucial role, for example, in generating free radicals and low-energy electrons in biological systems upon exposure to light, which may damage DNA strands and cause cancer.[12–14]

LiHe is also an interesting candidate to investigate the transfer of energy between far apart atoms. Although not as extended as He_2, the $^7Li^4He$ isotope and, in particular, $^6Li^4He$ are extremely huge and live mainly in the classical forbidden region. However, unlike for He_2, for LiHe, it is only necessary to excite helium and there is no need to ionize it in order to have ICD. As a result, there is no Coulomb explosion and bound cations can be detected, giving rise to a completely different appearance of ICD than in the He_2 case. The lowest optical excitation of helium is to the $1s2p\,^1P$ state, and the stored energy in the excited He* (21.22 eV at the asymptote)[15] is sufficient to ionize Li (5.39 eV at the asymptote).[15] The electronic state of the dimer in this case splits into a $^2\Sigma$ and a $^2\Pi$ state in accordance with the orientation of the $2p$ orbital with respect to the interatomic axis.

Helium nanodroplets doped with Li atoms were investigated recently experimentally and theoretically.[16,17] It was shown that upon excitation of He, using a photon energy of $h\nu$ = 21.6 eV, the doped droplet undergoes interatomic ionization processes. Since the excited He atom is embedded in a droplet, these processes occur out of the $1s2s\,^1S$ level (and partially out of the $1s2s\,^3S$ state) due to ultrafast relaxation, irrespective of the initial excitation level. It was shown that the process is predominantly driven by the charge-exchange process (unlike the energy transfer process discussed above), which is related to the Penning ionization mechanism.[16,17]

Herein, we are interested in the LiHe dimer for which the abovementioned relaxation process, after optical excitation to $He^*(1s2p\,^1P)$–Li, does not take place. In order to study ICD theoretically, it is essential to perform nuclear dynamics. This goal requires the potential energy curves of the resonances, i.e., of the decaying electronic states of the dimer, which are complex.[18] Complex potential energy curves (CPECs) corresponds to the position (real part) and width or lifetime (imaginary part) of the resonance states. In this paper, we present the CPECs of the LiHe in which helium is excited in to the $1s2p\,^1P$ state. They are calculated using the resonance via Padé (RVP) approach, in which real-space stabilization graphs are analytically dilated into the complex plane. The stabilization graphs are calculated with equation-of-motion coupled cluster (EOM-CC).[19,20] The employed basis set was determined and optimized for $He^*(1s2p\,^1P)$–Li in a previous publication.[21] The RVP approach was introduced,[22,23] benchmarked,[24] and successfully used to interpret cold chemistry experiments[25,26] by us. The method is, in particular, suitable for studying Feshbach and ICD resonances such as the $He^*(1s2p\,^1P)$–Li $^2\Sigma$ and $^2\Pi$ states.[24] The nuclear dynamics of these autoionization processes will be presented in a future work.

II. METHODS

A. The stabilization technique

Stabilization graphs are computed in the real space using standard (Hermitian) electronic structure methods. The metastable resonance states, which are located above the ionization threshold, are approximated as "bound states" embedded in the continuum. Within this technique, the eigenvalues are computed using a given set of finite basis functions (BFs) in which some of them are scaled by a real factor, α. Specifically, the scaling implies that the exponents of the selected BFs are divided by α. Typically, only the most diffuse functions are scaled.[27] This is done in a series of calculations in which α is continually varied. While for $\alpha < 1$, the spatial distribution of the basis set compresses and for $\alpha > 1$, it expands, typically, we employ the range $0.6 < \alpha < 2.0$ with $\alpha_i - \alpha_{i-1} = 0.04$, i.e., few tens of calculations. Since only part of the BFs (the most diffuse) are scaled, note that too small α values may cause linear dependency, while too large α values may cause gaps in the basis set.[21] A plot of the eigenvalues as a function of α is known as a stabilization graph.

Continuum and resonance states behave differently when a finite basis set is scaled. This behavior is attributed to the wavefunction associated with each state. The continuum states are associated with a delocalized wavefunction, whereas the resonance states are more localized in the interaction region.[18] Therefore, the resonance eigenvalues would not be affected strongly by a small compression and/or expansion of the basis set. On the contrary, continuum eigenvalues depend strongly on the scaling parameter. The regions where the continuum eigenvalues attempt to cross the resonance eigenvalues are known as the avoided crossings. (Note that the actual crossing occurs at the complex plane and is known as a branch-point or exceptional-point in the spectrum of the Hamiltonian.[28]) Input data for RVP calculations are taken from the "stable region," which is located between two avoided crossings.

B. The resonance via Padé (RVP) approach

Clearly, stabilization graphs present only an approximation to the resonance state's *positions*. In order to calculate the *complex* energies based on the stabilization technique, we carry out analytic dilation from the real axis into the complex plane. For that, we employ the RVP approach, which is based on the Padé approximant. In this method, single-level eigenvalues are used as input data for the analytic continuation, i.e., data from the stable (locally analytic) part of the stabilization graph. An analytic path from this stable region into the complex plane is formed, where the stationary points (SPs) along the path are identified as the resonance energies.[22] The association of SPs with resonance energies was first recognized via cusps in complex-scaling parameter trajectories.[29]

Generally, the stable part of a stabilization graph represents an energy function of a real scaling parameter, η, where $\eta = \alpha e^{i\theta}$ with $\theta = 0$. Within the Padé approximant, the energy function is fitted to a ratio between two polynomials,

$$E(\eta) = \frac{P(\eta)}{Q(\eta)}. \tag{1}$$

Practically, we use the Schlessinger point method[30] to generate a numerical expressionto $E(\eta)$. A set of N input variables, η_j's (=α_j's),

and their corresponding eigenvalues are chosen, from the stable part of the stabilization curves, and fitted to the truncated continued fraction,

$$C_M(\eta) = \cfrac{E(\eta_1)}{1 + \cfrac{z_1(\eta - \eta_1)}{1 + \cfrac{z_2(\eta - \eta_2)}{\ddots z_{M-1}(\eta - \eta_{M-1})}}}, \tag{2}$$

where the z_j coefficients are chosen by imposing the following condition:

$$C_M(\eta_j) = E(\eta_j),\ j = 1, 2, \ldots, M. \tag{3}$$

After determining the z_j coefficients, an analytical dilation is performed by evaluating $C_M(\eta)$, where $\eta = \alpha e^{i\theta}$ (with $\theta \neq 0$) is now complex. The complex resonance energies are identified as SPs in the complex plane, $E(\alpha_{SP}, \theta_{SP})$. These SPs satisfy the conditions[29]

$$\left.\frac{dE}{d\alpha}\right|_{\theta=\theta_{SP}}^{\alpha=\alpha_{SP}} = 0\,, \quad \left.\frac{dE}{d\theta}\right|_{\theta=\theta_{SP}}^{\alpha=\alpha_{SP}} = 0.$$

However, satisfying these conditions is a complicated task, which can be fulfilled, for example, graphically by looking for cusps in the associated α- and θ-trajectories.[22] Therefore, the more general condition,

$$\left.\frac{dE}{d\eta}\right|_{\eta=\eta_{SP}} = 0,$$

is used, for which we obtain algebraic solutions.[31] However, the solutions of the general condition incline to yield, in addition to the resonance energies, false SPs, i.e., unphysical solutions.[31]

C. The clusterization technique

Input data for RVP should be taken from the stable part of the stabilization graph.[22] However, this is not a clear-cut definition to the proper dataset that is suitable for RVP. The RVP complex energies, associated with the SPs, depend on the choice of the input data.[24] That is, RVP calculations using different parts of the "stable region" as input may yield very different complex energies. The clusterization technique[24] aims to tackle this issue. Since the analytical continuation step within the RVP calculation takes only few seconds on a standard personal computer,[31] it is possible to perform hundreds of RVP calculations, where the association of the physical-resonance energy with certain RVP SPs takes a statistical nature.

Once in possession of a stabilization graph, we identify the stable region, and then, we scan it and generate all possible input sets that are contained in this region. We use the "whole stable region" as the initial RVP input set. The "whole stable region" is the region in which the energy difference between consecutive points, $E(\alpha_{i+1}) - E(\alpha_i)$, is relatively small. Then, we start to scan and eliminate data points from the "whole stable region" to generate all possible sets of the RVP input. For each such input set, we compute the RVP SPs. In each RVP calculation, we look for SPs in the complex plane by varying the scaling parameter $\eta = \alpha e^{i\theta}$. α should cover the entire stabilization graph, and θ should not exceed $\pi/4$; this is analogous to the complex scaling approach, in which one wants to keep the scaled kinetic operator and the real-part of the potential as positive definite operators.[18] Finally, we identify SP clusters in the four-dimensional space of the energy and scaling parameters: ReE, ImE, α, and θ. The identified clusters are classified, and their quality is determined by the standard deviation (STD) of the calculated energies and scaling parameters. The average (mean) value of the identified cluster is identified as the RVP complex resonance energy.[24]

III. COMPUTATIONAL DETAILS

The electronic He*($1s2p\,^1P$)–Li ($^2\Sigma$ and $^2\Pi$) states are calculated within the spin-flip variant of EOM-CC (EOM-SF-CC).[19] We note that the spin-flip variant was chosen since the excitation-energy (EOM-EE-CC) one fails to converge for these highly-excited states. The computational scheme is presented in Fig. 1, with the reference state on the left side and the target multi-configuration state on the right. The reference state employed within the EOM-SF-CC calculation is the high-spin quartet Li($1s^2 2s\alpha$)–He($1s\alpha 2p_{x/y}\alpha$) configuration. The target-state is presented by the two most dominant determinants (as at the asymptote), where at shorter inter-atomic distances, additional determinants become important too. For calculating the CPEC of the $^2\Pi$ state, we use the singles and doubles truncation (EOM-CCSD), while for the $^2\Sigma$ state, we also include triples corrections via EOM-CCSD(dT).[32] The reason for this is that the dominated determinants in the $^2\Sigma$ resonance also include double-excitations relative to the reference state (Fig. 1). Finally, the cation in its ground state is calculated with CCSD(T). These calculations are done within the *Q-Chem* electronic-structure package.[33]

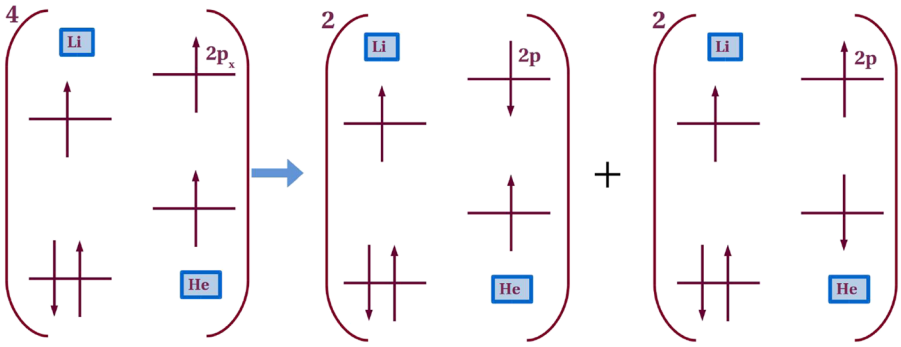

FIG. 1. Reference-state → EOM-SF-CC → target-state.

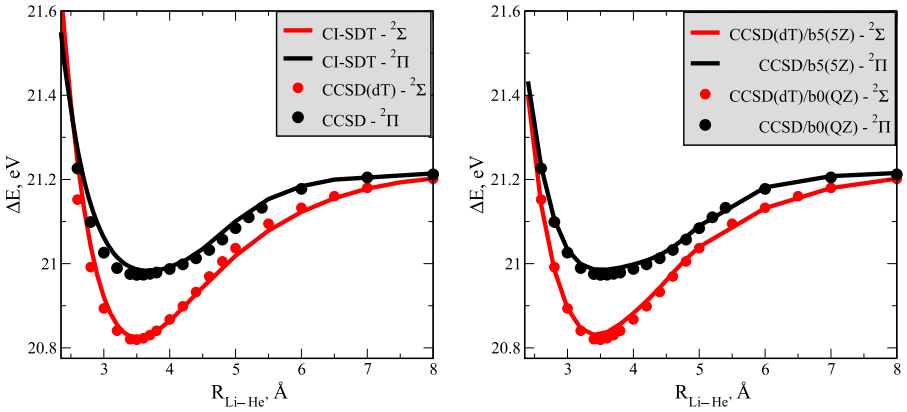

FIG. 2. Convergence of the approximated position (calculated as "bound states") of the $^2\Sigma$ and $^2\Pi$ resonance states. Left—convergence with respect to the many-electron basis set, EOM-CCSD/b0($^2\Pi$), and EOM-CCSD(dT)/b0($^2\Sigma$) vs CI-SDT/b0. Right—convergence with respect to the size of the one-electron basis set and the modified cc-pV5Z (b5) vs cc-pVQZ (b0). ΔE (in eV) represents the difference between the energy of the resonance states and the LiHe ground state energy at the asymptote.

The employed atomic-center basis sets were optimized and reported in Ref. 21; these are modified cc-pVQZ basis sets. The basis set used for calculating the initial real PECs is referred to as b0, where it is modified by adding two and three diffuse functions to Li and He, respectively. The additional diffuse functions are *s*- and *p*-type functions. b0 has 7*s*/5*p*/3*d*/2*f* functions centered on Li and 7*s*/6*p*/2*d*/1*f* functions centered on He. This basis set accurately describes the atomic He excitation $1s^2 \rightarrow 1s2p$. In addition, convergence with respect to the principle part of the basis was examined by using a modified cc-pV5Z basis set, referred to as b5 below. It is obtained by adding two and three diffuse functions to Li and He, respectively. The additional diffuse functions are *s*- and *p*-type functions. b5 has 8*s*/7*p*/4*d*/2*f* functions centered on Li and 8*s*/8*p*/2*d*/1*f* functions centered on He. For the calculations of the resonance CPECs, the bases are expended by adding diffuse BFs to the b0 basis set. Bases C and b2 are used for the $^2\Sigma$ and $^2\Pi$ states, respectively. They include 9*s*/8*p*/3*d*/2*f* functions centered on Li (the He-centered BFs are fixed for all bases). They differ in the exponents of types *d* and *f* (see Ref. 21 for details). The stabilization graphs are obtained by scaling the most diffuse 2*s*/2*p*/2*d*/2*f* basis function centered on Li.

IV. RESULTS

The excited $^2\Sigma$ and $^2\Pi$ resonance states of the Li–He* dimer, in which Li is in its ground state and He* is in an excited state, are investigated. The He* configuration in the $^2\Sigma$ and $^2\Pi$ states is $1s^1 2p_z^1$ and $1s^1 2p_x^1/1s^1 2p_y^1$, respectively, where the molecular axis is in the *z* direction. Our goal is to present their CPECs, which will be used in future work for describing the nuclear dynamics of the autoionization reaction. First, before going into the complex plane, we are considering these resonance states as bound states in the continuum. The right panel of Fig. 2 presents the convergence of the "bound" state's potential energy curves (PECs) with respect to the one-electron basis set. It presents the convergence between two bases, b0 and b5, which are based on cc-pVQZ and cc-pV5Z, respectively (see Sec. III for details). The left panel of Fig. 2 presents the convergence of these PECs with respect to the many-body basis set. It compares EOM-CCSD for the $^2\Pi$ state and EOM-CCSD(dT) for the $^2\Sigma$ state with configuration interaction at the singles, doubles, and full triples (CI-SDT). The dominated determinants in the $^2\Sigma$ resonance, unlike for the $^2\Pi$ state, also include double-excitations relative to the reference state (see Fig. 1); therefore, inclusion of perturbative triples correction is mandatory. Indeed, the PEC of the $^2\Sigma$ resonance state at the EOM-CCSD level (not shown) appears incorrectly above the $^2\Pi$ PEC. Note that CI-SDT is practically the full CI that eliminates the correlation effects of the two Li($1s^2$) electrons, which are negligible. The convergence presented in Fig. 2, with respect to the one-electron and many-electrons bases, is satisfactory.

Figure 3 shows that the $^2\Sigma$ and $^2\Pi$ states are resonance states by plotting them along with the $LiHe^+$ PEC. Note that at the asymptote, the He* curve yields 21.215 eV and the cation curve yields 5.365 eV in agreement with the NIST values for the atomic He*($1s2p\,^1$S) excitation, 21.218 eV, and with the ionization potential

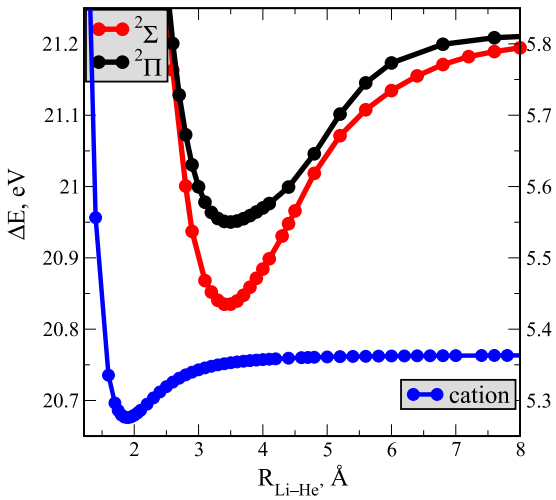

FIG. 3. Potential curves relevant for the ICD process. The $^2\Sigma$ and $^2\Pi$ resonances [EOM-CCSD(dT)/C and EOM-CCSD/b2, respectively, where the energy scale corresponds to the left *y*-axis] are above the cation curve shown in blue [CCSD(T)/b0, energy scale corresponds to the right *y*-axis]. ΔE (eV) represents the difference from the Li–He ground state energy at the asymptote. Note that at the asymptote, the cation curve corresponds to the ionization energy of Li, and the resonance curves correspond to the excitation energy into He*($1s2p\,^1$P).

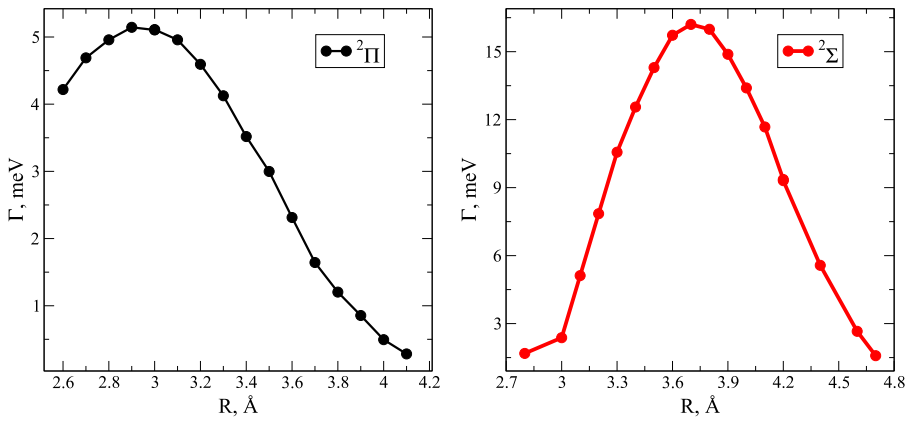

FIG. 4. The RVP EOM-CCSD widths (in meV) of the $^2\Pi$ (left panel; using basis set b2) and $^2\Sigma$ (right panel; using basis set C) resonance states.

of Li, 5.392 eV.[15] Clearly, the $^2\Sigma$ and $^2\Pi$ PECs are for all internuclear distances above the cation one, i.e., above the ionization threshold. Note that the energy scale of the resonance curves is on the left *y*-axis, while that of the cation curve is on the right *y*-axis. Therefore, these states are resonance states, and the proper way to treat them is in the complex plane, within non-Hermitian quantum mechanics.[18]

For this reason, we use the RVP method, which is suitable for calculating autoionization Feshbach states and ICD resonances such as the $^2\Sigma$ and $^2\Pi$ states.[24] We calculate stabilization graphs at each interatomic distance for both states. Examples for such stabilization graphs can be found in Figs. 7 and 11 of Ref. 21 for the $^2\Pi$ (using basis set b2) and $^2\Sigma$ (using basis set C) states at $R = 3.4$ Å, respectively. Once the stabilization graphs are calculated, we use their stable part as input data for fitting a Padé function, which is used for analytical dilation into the complex plane. Then, we look for SPs in the complex plane. We use the clusterization technique to identify the most statistically suitable group of SPs, which are associated with the resonance states. Examples for specific clusterization procedures are described in Ref. 24 in Fig. 8 for the $^2\Pi$ (using b2) and in Fig. 7 for the $^2\Sigma$ (basis set C) states, respectively.

Figure 4 presents the width, $\Gamma = -2\mathrm{Im}E$, of the $^2\Pi$ and $^2\Sigma$ states as a smooth function of the interatomic distance. These widths are obtained by the RVP/clusterization described above, and they are calculated at the EOM-CCSD level of theory. RVP also provides the corrected position (i.e., the real part of the resonance energy) relative to the approximated "bound state" calculations; however, the difference in our case is negligible, less than 0.02 eV. Note that RVP cannot be used at smaller or larger interatomic distances than the ones presented in Fig. 4 since the width becomes too small to be distinguished from the noise and it becomes difficult to identify resonances. Figure 5 presents the perturbative triples corrections, within EOM-CCSD(dT), for the width of the $^2\Sigma$ state and contrasts it with the EOM-CCSD results. The need to include triples in the calculations of the $^2\Sigma$ state is discussed in Sec. III. The triples corrections lower the size of Γ(R) between R = 3 Å and R = 4.5 Å; out of this range, their effect is small. We note that inclusion of triples corrections within EOM-CCSD(dT) is difficult. The RVP calculations become less stable, and at some interatomic distances, we cannot identify the complex energy of the system (the stabilization graph become less smooth, and as a result, the STD of the RVP width becomes too large). This is a result of using perturbative triples corrections, and we expect that including the full triples would again stabilize the RVP calculations (as in the singles and doubles calculations); however, such calculations for so highly excited states are not feasible nowadays. Nevertheless, we obtain sufficiently many satisfactory RVP solutions (blue points in Fig. 5) to generate a smooth Γ(R) function by fitting these points to Padé.

The shape of the Γ(R) functions is unusual. Starting at the small internuclear distance, Γ's first unexpectedly increase with growing distance and then, after reaching a maximum, decrease as expected for larger distances. Since metastable states of He, in particular, ^3S states, are frequently used in ionizing a target system via collisions (Penning ionization), it is interesting to compare the respective

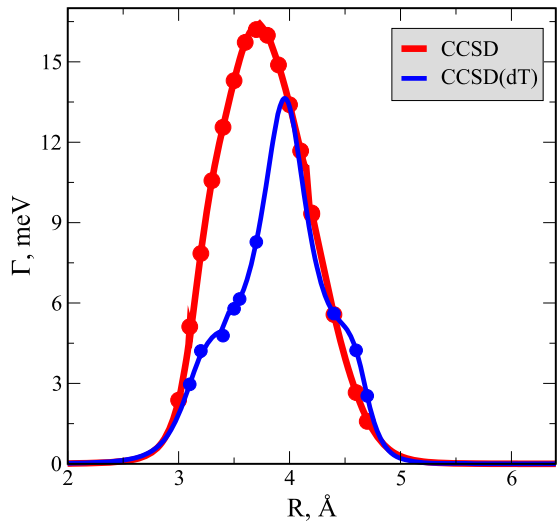

FIG. 5. A comparison of the widths (in meV) of the $^2\Sigma$ resonance state computed at the EOM-CCSD and EOM-CCSD(dT) levels of theory using basis set C. The calculated data points are presented, and the curved line is obtained by fitting them to a Padé function.

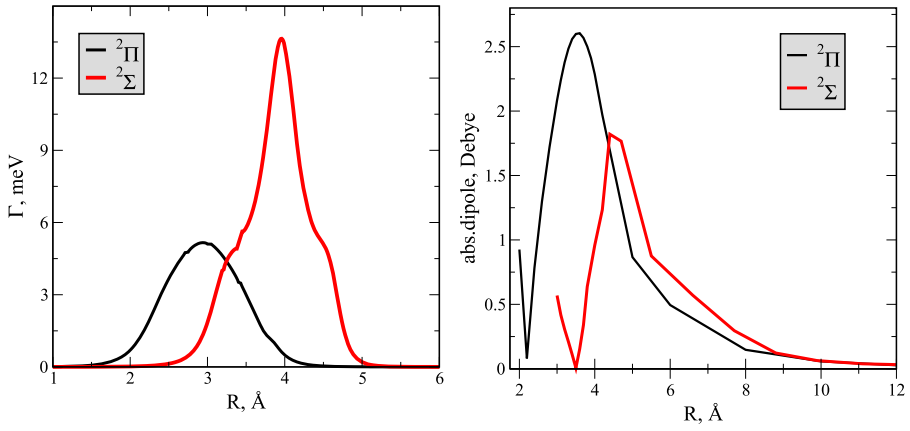

FIG. 6. Comparable behavior of the widths (left panel, in meV) and of the absolute value of the permanent dipole functions (right panel, calculated as "bound states" in Debye) of the $^2\Sigma$ and $^2\Pi$ resonance states. The quantities of $^2\Sigma$ and $^2\Pi$ states are calculated with [EOM-CCSD(dT)/C] and (EOM-CCSD/b2), respectively.

width functions. The Penning width function at R = 0 is large and known to decrease substantially with R,[25,26,34] while the ICD width functions computed here have a totally different appearance (Figs. 4 and 5). Note that ICD is collision free and, according to Eq. (4), it is, in principle, a long range process, which becomes faster as the radiative decay width of He^* becomes larger. In Penning ionization, however, traditionally, one is interested in resonance states that are characterized by a relatively small radiative width in order to be able to carry out collision experiments as, for example, in the collision of $He^*(2^3S)$ with H_2[25] and with Li.[17] Interestingly, the behavior of Γ(R) corresponds to the behavior of the absolute-value of the permanent dipole. The left panel of Fig. 6 depicts the computed widths of the $^2\Pi$ and $^2\Sigma$ resonance states, and the right panel depicts their permanent approximated dipoles (calculated as "bound" states with EOM-CCSD and the respective basis sets). Clearly, the behavior of the absolute-value of the permanent dipole is also involved and resembles that of the Γ(R) functions, where the peaks of the dipole functions are at slightly larger interatomic distances than the peaks of Γ(R). Thus, the changes in the width function are correlated with the changes in the permanent dipole functions. This is interesting since both the width and the permanent dipole are inherent electronic properties of the respective states.

Our purpose is to present CPECs that are suitable for the description of the nuclear dynamics of the associated ICD processes. Since $^7Li^4He$ and $^6Li^4He$ are halo systems (see the Introduction), we need to arrive at CPECs valid also at larger interatomic distances than discussed above. Therefore, we extrapolate the computed CPECs into larger distances in the following manner. An analytical expression for the general behavior of ICD widths at very large interatomic distances is given in Ref. 35 (see also earlier work in Ref. 36),

$$\lim_{R\to\infty}\Gamma=\frac{c}{2\pi\Delta E}\frac{P^{He^*}(M_L^{He^*})S^{He^*}(\Delta E)\sigma^{Li}(\Delta E)}{R^6}, \tag{4}$$

where c is the speed of light. $P^{He^*}(M_L^{He^*})$ is the Clebsch–Gordan coefficient, which equals 3/4 and 1/4 for the $^2\Sigma$ and $^2\Pi$ states, respectively[35] (and $M_L^{He^*}$ is the projection of the excited He^* state angular momentum). Therefore, $\Gamma_{^2\Pi}/\Gamma_{^2\Sigma}=4$.[35] $S^{He^*}(\Delta E)$ is the line strength (a function of the oscillator strength, which equals about 0.09208), and ΔE = 21.218 eV.[15] Using this oscillator strength, $S^{He^*}(\Delta E)$ becomes 0.5314 a.u. σ^{Li} is the photoionization cross section of Li, and according to Ref. 37, at ΔE = 21.218 eV, it equals 0.815 Mb. All in all, we obtain

$$\begin{aligned}\lim_{R\to\infty}\Gamma_{^2\Pi}&=6.756/R^6,\\ \lim_{R\to\infty}\Gamma_{^2\Sigma}&=27.0245/R^6,\end{aligned} \tag{5}$$

where $\Gamma_{^2\Pi}$ and $\Gamma_{^2\Sigma}$ are in meV and R is in Å. Once in possession of the asymptotic functions [Eq. (5)] and the RVP results (at relatively short interatomic distances; see the left panel of Fig. 6), we interpolate between them. Figure 7 presents the width of the $^2\Sigma$ and $^2\Pi$ resonance states up to 80 Å in log scale. Note that the real part of the CPECs is already rather flat at the distances computed and can be easily extrapolated into the sum of the atomic energies.

Finally, we wish to know at which interatomic distance does the asymptotic behavior begin. For that, we fit a power function to

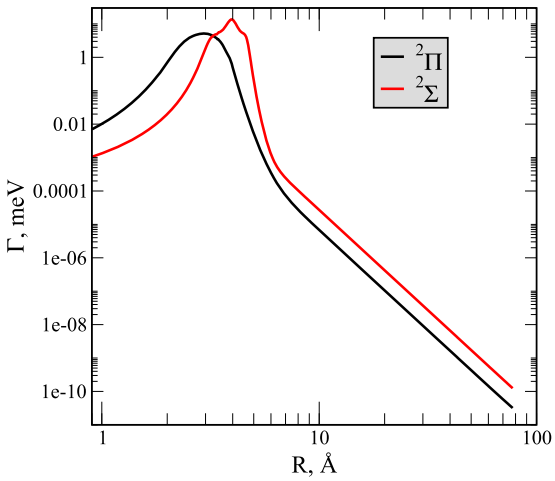

FIG. 7. Interpolation of the widths (in meV), between the RVP results (Fig. 6, left panel) and the asymptotic behavior [Eq. (5)], of the $^2\Sigma$ and $^2\Pi$ resonance states in logarithmic scale.

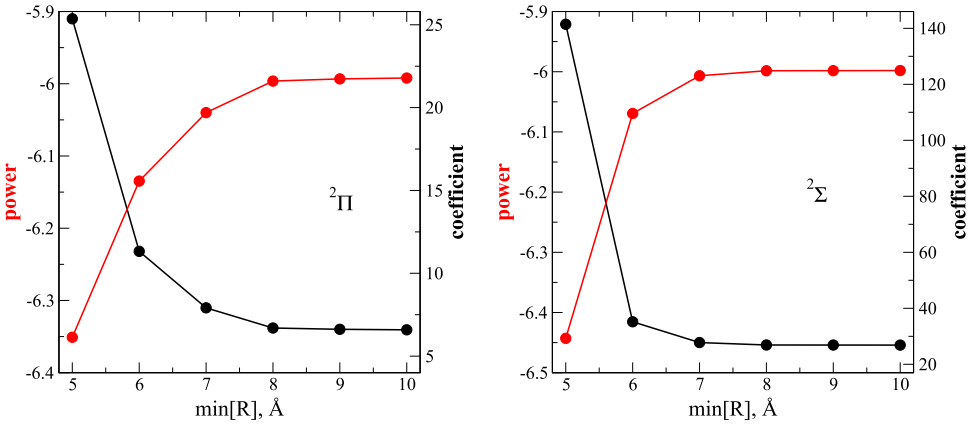

FIG. 8. Where does the asymptotic behavior begin? Numerical fitting to a power function of the Γ curves shown in Fig. 7. Left: $^2\Sigma$ and right: $^2\Pi$. The power (red) and coefficient (black) are obtained as a function of the minimal R, where the maximal R is fixed to 80 Å (see text for details). Asymptotically, $\Gamma_{^2\Pi} = 6.632/R^6$ and $\Gamma_{^2\Sigma} = 26.527/R^6$ {in meV and R is in Å [Eq. (5)]}. Therefore, the asymptote begins at 7 Å for $^2\Sigma$ and at 8 Å for $^2\Pi$.

the values of the Γ functions in Fig. 7 between the maximal distance (max[R] = 80 Å) and a variable minimal value, min[R]. Figure 8 presents the power (red and left *y*-axis) and the coefficient (black and right *y*-axis) as a function of min[R] for the $^2\Pi$ (left panel) and $^2\Sigma$ (right panel) states. We observe that the asymptotic behavior begins at 7 Å for $^2\Sigma$ and at 8 Å for $^2\Pi$ since below these min[R]'s, the power and coefficients start to deviate from the values in Eq. (5). This result is consistent with the analysis in Ref. 38, which showed that a reasonable distance in which the asymptotic behavior starts is roughly twice as large as the associated equilibrium distance.

V. SUMMARY

In this paper, we present *ab initio* complex potential energy curves of the He^*–Li in which helium is excited in to the $1s2p^1P$ state. The electronic states associated with $He^*(1s2p^1P)$–Li are $^2\Sigma$ and $^2\Pi$. These states are located above the ionization threshold of Li, and therefore, they are resonance states decaying by ICD to $He–Li^+$ and are characterized by having complex energies. To compute them, we use here the resonance via Padé (RVP) approach.[22–24] This approach uses real-space stabilization graphs as input data for analytical dilation into the complex plane. The stabilization graphs are calculated with EOM-CC, where the basis set used was optimized in a previous publication.[21] The method is, in particular, suitable for studying Feshbach and ICD states such as the $^2\Sigma$ and $^2\Pi$ resonance states.[24] Our purpose is to arrive at CPECs that are suitable for describing the nuclear dynamics of the associated ICD processes. Since He–Li is a halo system (see the Introduction), which extends well into the classical forbidden region, we interpolate between the RVP results (at relatively short interatomic distances) and an analytical expression for the behavior at large interatomic distances, which is given in Ref. 35. A numerical analysis shows that the asymptotic behavior of the $^2\Sigma$ and $^2\Pi$ states starts at $R > 7$ Å and $R > 8$ Å, respectively. The resulting CPECs will be used in future work, which is devoted to the nuclear dynamics of the associated ICD processes.

ACKNOWLEDGMENTS

This research was supported by the Israel Science Foundation (Grant No. 1661/19).

L.S.C. gratefully acknowledges funding from the European Research Council (Advanced Investigator Grant No. 692657).

A.B.-A. gratefully acknowledges the support of the Adams Fellowship Program of the Israel Academy of Sciences and Humanities.

DATA AVAILABILITY

The data that support the findings of this study are available from the corresponding author upon reasonable request.

REFERENCES

[1] B. Friedrich, Physics **6**, 42 (2013).
[2] N. Tariq, N. Al Taisan, V. Singh, and J. D. Weinstein, Phys. Rev. Lett. **110**, 153201 (2013).
[3] F. Luo, G. C. McBane, G. Kim, C. F. Giese, and W. R. Gentry, J. Chem. Phys. **98**, 3564 (1993).
[4] W. Schöllkopf and J. P. Toennies, Science **266**, 1345 (1994).
[5] A. S. Jensen, K. Riisager, D. V. Fedorov, and E. Garrido, Rev. Mod. Phys. **76**, 215 (2004).
[6] U. Kleinekathöfer, M. Lewerenz, and M. Mladenović, Phys. Rev. Lett. **83**, 4717 (1999).
[7] R. E. Grisenti, W. Schöllkopf, J. P. Toennies, G. C. Hegerfeldt, T. Köhler, and M. Stoll, Phys. Rev. Lett. **85**, 2284 (2000).
[8] N. Sisourat, N. V. Kryzhevoi, P. Kolorenč, S. Scheit, T. Jahnke, and L. S. Cederbaum, Nat. Phys. **6**, 508 (2010).
[9] L. S. Cederbaum, J. Zobeley, and F. Tarantelli, Phys. Rev. Lett. **79**, 4778 (1997).
[10] R. Santra, J. Zobeley, L. S. Cederbaum, and N. Moiseyev, Phys. Rev. Lett. **85**, 4490 (2000).
[11] N. Moiseyev, R. Santra, J. Zobeley, and L. S. Cederbaum, J. Chem. Phys. **114**, 7351 (2001).
[12] L. Sanche, Radiat. Prot. Dosim. **99**, 57 (2002).
[13] F. Trinter, M. S. Schöffler, H.-K. Kim, F. P. Sturm, K. Cole, N. Neumann, A. Vredenborg, J. Williams, I. Bocharova, R. Guillemin, M. Simon, A. Belkacem, A. L. Landers, T. Weber, H. Schmidt-Böcking, R. Dörner, and T. Jahnke, Nature **505**, 664 (2014).
[14] K. Gokhberg, P. Kolorenč, A. I. Kuleff, and L. S. Cederbaum, Nature **505**, 661 (2014).
[15] A. Kramida, Yu. Ralchenko, J. Reader, and NIST ASD Team, NIST Atomic Spectra Database (ver. 5.7.1) (Online), available at https://physics.nist.gov/asd (April 16, 2015), National Institute of Standards and Technology, Gaithersburg, MD, 2019.

[16]D. Buchta, S. R. Krishnan, N. B. Brauer, M. Drabbels, P. O'Keeffe, M. Devetta, M. Di Fraia, C. Callegari, R. Richter, M. Coreno *et al.*, J. Phys. Chem. A **117**, 4394 (2013).
[17]L. Ben Ltaief, M. Shcherbinin, S. Mandal, S. R. Krishnan, A. C. LaForge, R. Richter, S. Turchini, N. Zema, T. Pfeifer, E. Fasshauer, N. Sisourat, and M. Mudrich, J. Phys. Chem. Lett. **10**, 6904 (2019).
[18]N. Moiseyev, *Non-Hermitian Quantum Mechanics* (Cambridge University Press, Cambridge, 2011).
[19]A. I. Krylov, Phys. Chem. **59**, 433 (2008).
[20]R. J. Bartlett and M. Musiał, Rev. Mod. Phys. **79**, 291 (2007).
[21]A. Landau, Mol. Phys. **117**, 2029 (2019).
[22]A. Landau, I. Haritan, P. R. Kaprálová-Žďánská, and N. Moiseyev, J. Phys. Chem. A **120**, 3098 (2016).
[23]A. Landau, D. Bhattacharya, I. Haritan, A. Ben-Asher, and N. Moiseyev, *Advances in Quantum Chemistry* (Elsevier, 2017), Vol. 74, pp. 321–346.
[24]A. Landau and I. Haritan, J. Phys. Chem. A **123**, 5091 (2019).
[25]D. Bhattacharya, A. Ben-Asher, I. Haritan, M. Pawlak, A. Landau, and N. Moiseyev, J. Chem. Theory Comput. **13**, 1682 (2017).
[26]D. Bhattacharya, M. Pawlak, A. Ben-Asher, A. Landau, I. Haritan, E. Narevicius, and N. Moiseyev, J. Phys. Chem. Lett. **10**, 855 (2019).
[27]A. Landau, I. Haritan, P. R. Kaprálová-Žďánská, and N. Moiseyev, Mol. Phys. **113**, 3141 (2015).
[28]N. Moiseyev and S. Friedland, Phys. Rev. A **22**, 618 (1980).
[29]N. Moiseyev, S. Friedland, and P. R. Certain, J. Chem. Phys. **74**, 4739 (1981).
[30]L. Schlessinger, Phys. Rev. **167**, 1411 (1968).
[31]I. Haritan and N. Moiseyev, J. Chem. Phys. **147**, 014101 (2017).
[32]P. U. Manohar and A. I. Krylov, J. Chem. Phys. **129**, 194105 (2008).
[33]Y. Shao *et al.*, Mol. Phys. **113**, 184 (2015).
[34]W. H. Miller and H. Morgner, J. Chem. Phys. **67**, 4923 (1977).
[35]K. Gokhberg, S. Kopelke, N. Kryzhevoi, P. Kolorenč, and L. Cederbaum, Phys. Rev. A **81**, 013417 (2010).
[36]K. Gokhberg, A. B. Trofimov, T. Sommerfeld, and L. S. Cederbaum, Europhys. Lett. **72**, 228 (2005).
[37]R. D. Hudson and V. L. Carter, J. Opt. Soc. Am. **57**, 651 (1967).
[38]V. Averbukh, I. B. Müller, and L. S. Cederbaum, Phys. Rev. Lett. **93**, 263002 (2004).